Genetic and ICP Laser Point Matching for 2D Mobile Robot Motion Estimation *

Jorge L. Martínez, Javier González, Jesús Morales,
Anthony Mandow and Alfonso J. García-Cerezo

Dept. of System Engineering and Automation
University of Málaga
Plaza El Ejido s/n, 29013-Málaga, Spain
Phone: (+34) 952 131408. Fax: (+34) 952 131413.
E-mail: jlmartinez@uma.es

Abstract

The paper reports on mobile robot motion estimation based on matching points from successive two-dimensional (2D) laser scans. This ego-motion approach is well suited to unstructured and dynamic environments because it directly uses raw laser points rather than extracted features. We have analyzed the application of two methods that are very different in essence: i) A 2D version of Iterative Closest Point (ICP), which is widely used for surface registration; ii) A Genetic Algorithm (GA), which is a novel approach for this kind of problem. Their performance in terms of real-time applicability and accuracy has been compared in outdoor experiments with non-stop motion under diverse realistic navigation conditions. Based on this analysis, we propose a hybrid GA-ICP algorithm that combines the best characteristics of these pure methods. The experiments have been carried out with the tracked mobile robot Auriga-α and an on-board 2D laser scanner.

1

1   Introduction

The aim of motion estimation is to capture the short-term behavior of mobile robots from sensor data. This information is useful for low-level control, for shaping the followed trajectory, and for kinematic model identification. Ego-motion estimation is essential for many field applications because, as opposed to pose estimation, it is a relative scheme that does not rely on an absolute world frame. Usually, this is computed by dead-reckoning, which comprises odometry and inertial sensors (Borenstein et al., 1997). These provide acceptable accuracy for sufficiently small steps, but their estimate can be improved if external sensor data is also considered.

This paper focusses on motion estimation by means of 2D laser point matching. On-board laser scanners have become common in mobile robotics due to a substantial increase in performance and a decrease in cost. Each scan provides a precise contour of the surrounding environment, so motion can be estimated by finding a correspondence between successive laser scans. Three-dimensional scanners are increasingly being used for off-road navigation, but two-dimensional range-finders are by large the most widely used ones for mobile robot operation on approximately flat terrains.

Scan matching, or registration, can be defined as finding the translation and rotation of a scan contour in such a way that a maximum overlap occurs with either a known map (i.e., position estimation) or a previous scan (i.e., motion estimation). Dead-reckoning can be employed to provide an initial estimation for this search. It must be noted that the integration of motion estimations (e.g., when applied to global localization or map building) inevitably leads to unbounded growth of pose uncertainty during navigation.

The application of scan matching methods for motion estimation can be broadly classified into three different categories:

1. Feature based techniques that discern distinctive geometrical patterns, such as line segments (González et al., 1994), corners (Shaffer et al., 1992) or edges (Weber et al., 2002), from the laser readings. Computation of these features can be a hard burden for ego-motion estimation.

2. Compact data methods that extract mathematical properties from range measurements such as histograms (Weiß et al., 1994), motion fields (González and Gutiérrez, 1999) or principal eigenvectors (Crowley et al., 1998). These characteristics can be very sensitive to measurement noise and moving objects in the sensed environment.

3. Point matching techniques that directly establish correspondences between spatial points from two laser scans. These are well suited for

motion estimation in unstructured and dynamic environments because they directly use raw laser data. Exact point correspondence is impossible due to sensor limitations, so matching is usually regarded as an optimization problem where the maximum expected precision is intrinsically limited by the working environment and by the rangefinder performance.

Different optimization-based techniques have been proposed for point matching methods, such as a direct-descent technique denominated Iterative Closest Point (ICP) (Chen and Medioni, 1991), (Besl and McKay, 1992), (Zhang, 1992), Gradient Computation (GC) (Neugebauer, 1997), (Fitzgibbon, 2001), (Thrun et al., 2000), Evolutionary Programming (EP) (Agrawal et al., 1994), Simulated Annealing (SA) (Blais and Levine, 1995), and, recently, a Genetic Algorithm (GA) (Martínez, 2003). Among them, the ICP procedure is the most popular because of its simplicity and effectiveness, and many variants have been proposed (Rusinkiewicz and Levoy, 2001). GC is based on calculating gradients of either probabilistic (Thrun et al., 2000) or squared-error (Neugebauer, 1997), (Fitzgibbon, 2001) cost functions. Finally, the EP, SA and GA methods introduce a stochastic component in the search of either the correspondence of points (Agrawal et al., 1994) or the whole pose (Blais and Levine, 1995), (Martínez, 2003).

Point correspondences can be computed either in polar (Neugebauer, 1997), (Thrun et al., 2000), (Blais and Levine, 1995), (Martínez, 2003) or cartesian (Chen and Medioni, 1991), (Besl and McKay, 1992), (Zhang, 1992), (Fitzgibbon, 2001), (Agrawal et al., 1994) coordinates. The latter strategy can be accelerated for large amounts of data by using closest point caching or multi-dimensional binary search trees (Zhang, 1992), which use information from previous matching tentatives. Moreover, unmatchable points can disrupt the optimization process if included in the cost function, so an adaptive statistical threshold can be used to discard outliers (Zhang, 1992), (Fitzgibbon, 2001).

In this paper, we have analyzed two essentially different point matching techniques for motion estimation: a fast 2D version of ICP, a local-scope optimizer which is the most widely used registration algorithm for 3D surfaces, and the GA method, a wide-scope technique which constitutes a novel stochastic approach for scan matching. Then, we propose a hybrid GA-ICP algorithm that combines the best characteristics of these methods. Comparative experimental results have been obtained with the tracked vehicle Auriga-α equipped with a commercial scanner.

The rest of the paper is organized as follows. In the next section, we enunciate the 2D laser point matching problem, we review the ICP and GA

methods, and we propose a hybrid GA-ICP solution. Subsequently, in section 3, these techniques are compared based on non-stop motion outdoor experiments under diverse realistic navigation conditions with the Auriga-α mobile robot. Finally, the conclusions and future work are outlined in section 4.

2   The 2D laser point matching problem

A laser scanner mounted on a vehicle generates a light beam that rotates in a horizontal plane parallel to the ground. Thus, a range scan at discrete time k can be defined as a set of points $\{\mathbf{q}_k\}$ which is represented in polar coordinates as a coupled list of distances and angles $\{(d_k, \alpha_k)\}$ that correspond to the successive intersections of the laser ray with the closest objects in the surroundings.

The scan angles are arranged consecutively and they are evenly spaced with a certain angular resolution ρ. The scanning sequence is indexed by j, which represents an integer between 0 and a maximum value N. If Φ denotes the field of view, N is given by Φ/ρ for partial field-of-view scans and by $(\Phi/\rho) - 1$ for complete circular scans (i.e., $\Phi = 360°$).

Let XY_k be a coordinate system attached to the rangefinder at discrete time k. Assuming that the X axis is aligned with the laser beam at $\alpha_k(0) = 0°$ (see Fig. 1), then:

$$\alpha_k(j) = \rho\, j \tag{1}$$

and the cartesian coordinates of the jth scanned point $\mathbf{q}_k(j)$ are:

$$
\begin{aligned}
x_k(j) &= d_k(j)\cos(\alpha_k(j)) \\
y_k(j) &= d_k(j)\sin(\alpha_k(j))
\end{aligned}
\tag{2}
$$

When in motion, two consecutive scans at discrete instants k and $k+1$ will be recorded from different poses of the vehicle. Thus, $\{\mathbf{q}_k\}$ and $\{\mathbf{q}_{k+1}\}$ will be expressed in polar coordinates on the laser frames at those instants, denoted by XY_k and XY_{k+1}, respectively. Both frames are defined with respect to an arbitrary global coordinate system.

In order to find correspondences between both scans, $\{\mathbf{q}_{k+1}\}$ must be projected onto the XY_k frame, which results in $\{\hat{\mathbf{q}}_k\}$ according to a tentative transformation T_k (see Fig. 2). T_k is composed of the relative displacements $(\Delta x, \Delta y)$ and the rotation increment $\Delta\phi$ between XY_k and XY_{k+1}.

Cartesian coordinates for $\{\hat{\mathbf{q}}_k\}$ are obtained as:

$$
\begin{bmatrix} \hat{x}_k(j) \\ \hat{y}_k(j) \end{bmatrix} = \begin{bmatrix} \cos(\Delta\phi) & -\sin(\Delta\phi) \\ \sin(\Delta\phi) & \cos(\Delta\phi) \end{bmatrix} \begin{bmatrix} x_{k+1}(j) \\ y_{k+1}(j) \end{bmatrix} + \begin{bmatrix} \Delta x \\ \Delta y \end{bmatrix}
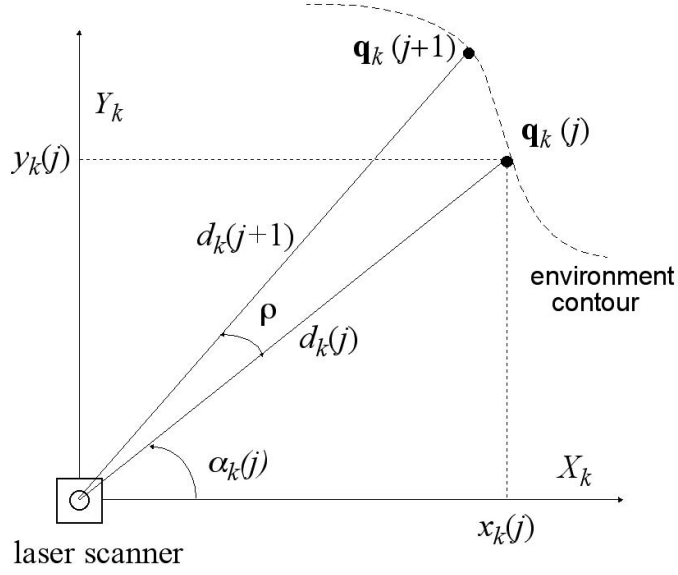\tag{3}
$$

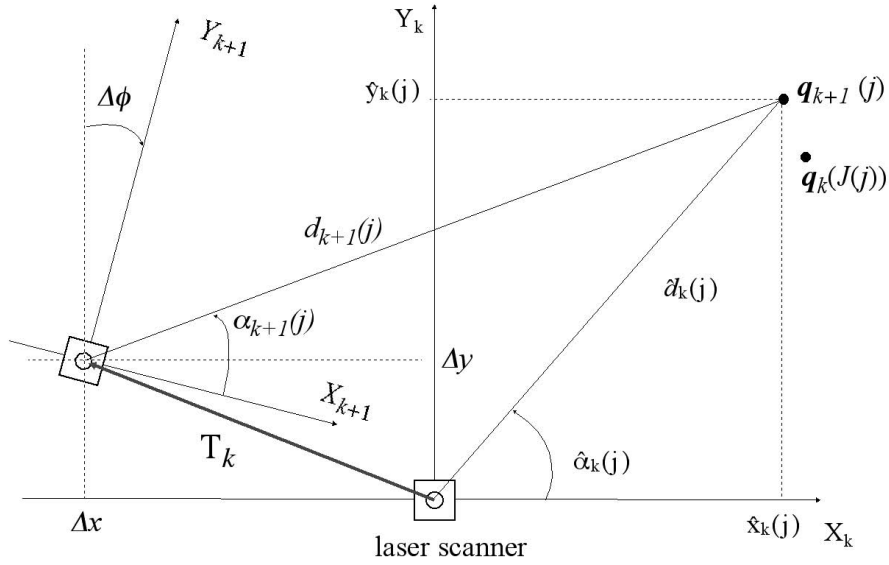Figure 1: Cartesian and polar coordinates of the $\mathbf{q}_k(j)$ point.

Figure 2: Projection of $\mathbf{q}_{k+1}(j)$ onto the XY_k frame.

Similarly, the projected polar coordinates for $\{\hat{\mathbf{q}}_k\}$ can be computed as:

$$\hat{\alpha}_k(j) \;=\; \Delta\phi + \arctan\left(\frac{y_{k+1}(j) + \Delta y}{x_{k+1}(j) + \Delta x}\right) \tag{4}$$

$$\hat{d}_k(j) \quad = \quad \sqrt{(x_{k+1}(j) + \Delta x)^2 + (y_{k+1}(j) + \Delta y)^2}$$

Assuming a given transformation estimation T_k, let us define the correspondence index function as $J(j)$ if the projection $\hat{\mathbf{q}}_k(j)$ of point $\mathbf{q}_{k+1}(j)$ corresponds with $\mathbf{q}_k(J(j))$. A match error function $e_{T_k}(j)$ can then be defined for each pair of matched points:

$$e_{T_k}(j) = e_{T_k}[\hat{\mathbf{q}}_k(j), \mathbf{q}_k(J(j))] \tag{5}$$

Unmatchable points can be discarded by defining a boolean function for outliers detection:

$$p_{T_k}(j) = \begin{cases} 0 & \text{if } |e_{T_k}(j)| \geq E \\ 1 & \text{otherwise} \end{cases} \tag{6}$$

given a correspondence threshold E. Consequently, the number n_{T_k} of valid correspondences is given by:

$$n_{T_k} = \sum_{j=0}^{N} p_{T_k}(j) \tag{7}$$

and the ratio that shows the degree of overlap of any possible transformation is:

$$P_{T_k} = \frac{n_{T_k}}{N + 1} \tag{8}$$

Exact correspondence of points from different scans is impossible due to a number of facts: deformation caused by vehicle motion, spurious ranges, random noise, terrain unevenness, mixed pixels, occluded areas, discretized angular resolution, moving objects, etc. Then, scan matching can be thought of as an optimization problem for determining a 2D transformation that minimizes a well-grounded matching criterion I_{T_k}.

A general matching index I_{T_k} for a given transformation T_k can be formulated by accumulating the matching errors and dividing this sum by n_{T_k} to normalize and by P_{T_k} to penalize low correspondence rates, that is:

$$I_{T_k} = \frac{\sum_{j=0}^{N} [p_{T_k}(j) \, e_{T_k}(j)]}{n_{T_k} \, P_{T_k}} \tag{9}$$

This expression represents the cost function to be iteratively minimized by point matching methods. A description of the ICP and GA methods can be found next. They mainly differ in the search procedure, in the definition of the match error function e_{T_k}, and in the adjustment of the outlier threshold E. After that, a hybrid GA-ICP approach is proposed.

2.1 Iterative closest point algorithm (ICP)

In spite of its popularity, particularly for 3D surface registration (Chen and Medioni, 1991), (Besl and McKay, 1992), (Zhang, 1992), (Rusinkiewicz and Levoy, 2001), including 3D SLAM (Surmann et al., 2004), only a few applications of ICP have been reported for 2D mobile robot motion estimation and always in combination with other methods (Lu and Milios, 1997), (Madhavan et al., 1998). Since our aim is to use the method for 2D scan matching, what follows is a description of a pure two-dimension point-to-point version of the algorithm (i.e. without tangent line calculations).

Firstly, T_k is initialized with the odometric motion estimation T_k^o before ICP starts four-step iterations. The first step calculates the cartesian coordinates of $\{\hat{\mathbf{q}}_k\}$ as the projection of $\{\mathbf{q}_{k+1}\}$ onto the XY_k frame according to Eq. (3).

The second step consists on computing the squared distances for every possible combination of $\{\hat{\mathbf{q}}_k\}$ and $\{\mathbf{q}_k\}$ points:

$$e(i\,,j) = (x_k(i) - \hat{x}_k(j))^2 + (y_k(i) - \hat{y}_k(j))^2 \qquad (10)$$

In the third step, ICP calculates the correspondence index function $J(j)$ based on minimum squared distances:

$$J(j) = m, \text{ if } e(m,j) = \min_{i=0}^{N}[e(i,\,j)] \qquad (11)$$

Thus, the match error function of Eq. (5) is given by:

$$e_{T_k}(j) = (x_k(J(j)) - \hat{x}_k(j))^2 + (y_k(J(j)) - \hat{y}_k(j))^2 \qquad (12)$$

and outliers detection is carried out with Eq. (6).

Finally, motion parameters are updated by minimizing Eq. (9) with the error definition of Eq. (12). This optimization can be solved analytically as follows:

$$\frac{\partial I_{T_k}}{\partial \Delta\phi} = 0 \Rightarrow \Delta\phi^{new} = \arctan\left(\frac{S_{x_k}S_{y_{k+1}} + n_{T_k}S_{y_k x_{k+1}} - n_{T_k}S_{x_k y_{k+1}} - S_{x_{k+1}}S_{y_k}}{n_{T_k}S_{x_k x_{k+1}} + n_{T_k}S_{y_k y_{k+1}} - S_{x_k}S_{x_{k+1}} - S_{y_k}S_{y_{k+1}}}\right)$$

$$\frac{\partial I_{T_k}}{\partial \Delta x} = 0 \Rightarrow \Delta x^{new} = \frac{S_{x_k} - \cos\left(\Delta\phi^{new}\right)S_{x_{k+1}} + \sin\left(\Delta\phi^{new}\right)S_{y_{k+1}}}{n_{T_k}} \qquad (13)$$

$$\frac{\partial I_{T_k}}{\partial \Delta y} = 0 \Rightarrow \Delta y^{new} = \frac{S_{y_k} - \sin\left(\Delta\phi^{new}\right)S_{x_{k+1}} - \cos\left(\Delta\phi^{new}\right)S_{y_{k+1}}}{n_{T_k}}$$

where the S terms stand for the following sums:

$$S_{x_k} = \sum_{j=0}^{N} [p_{T_k}(j)\, x_k(J(j))] \qquad S_{x_{k+1}} = \sum_{j=0}^{N} [p_{T_k}(j)\, x_{k+1}(j)]$$

$$S_{y_k} = \sum_{j=0}^{N} [p_{T_k}(j)\, y_k(J(j))] \qquad S_{y_{k+1}} = \sum_{j=0}^{N} [p_{T_k}(j)\, y_{k+1}(j)] \qquad (14)$$

$$S_{x_k x_{k+1}} = \sum_{j=0}^{N} [p_{T_k}(j)\, x_k(J(j))\, x_{k+1}(j)] \quad S_{x_k y_{k+1}} = \sum_{j=0}^{N} [p_{T_k}(j)\, x_k(J(j))\, y_{k+1}(j)]$$

$$S_{y_k x_{k+1}} = \sum_{j=0}^{N} [p_{T_k}(j)\, y_k(J(j))\, x_{k+1}(j)] \quad S_{y_k y_{k+1}} = \sum_{j=0}^{N} [p_{T_k}(j)\, y_k(J(j))\, y_{k+1}(j)]$$

This technique guarantees convergence to a local minimum that is close to the odometric estimation (Besl and McKay, 1992), which is not necessarily the optimal one (Zhang, 1992). Note that the most expensive computation of ICP is to find the closest points at each iteration.

The outlier threshold E is a critical parameter for the ICP algorithm. Some 3D implementations have proposed an adaptive statistical threshold (Zhang, 1992). To set up this parameter properly for 2D motion estimation, where less laser points are available and these are noisier, we propose a different approach. Since the registration error is reduced after each ICP iteration, E can be progressively decreased from E_{max} for the first iteration to E_{min} in the last one.

The value of E_{max} can be characterized from experimental calibration of odometric uncertainty (Muñoz et al., 1994). An upper bound of the expected odometric errors for each parameter of the transformation can be expressed as $\mathbf{b} = (b_x,\, b_y,\, b_\phi)$, which depends on the elapsed navigation time t between two consecutive scans. Then, E_{max} is calculated as a squared distance:

$$E_{max} = b_x^2 + b_y^2 \qquad (15)$$

As for E_{min}, the best possible registration should only depend on laser range errors. Provided that these are gaussian (Ye and Borenstein, 2002) with a standard deviation σ, squared match errors defined in Eq. (12) can be modeled as a chi-squared distribution (χ^2) of one degree of freedom. According to the percentage of this distribution, the squared threshold value that concentrates 99% of valid point correspondences is:

$$E_{min} = (\chi_{0.99}^2)^2 = (6.63\,\sigma)^2 \qquad (16)$$

2.2 Genetic algorithm (GA)

GAs provide a derivative-free stochastic optimization tool, where each point in a solution space is encoded into a bit string (chromosome) and is associated with a fitness value according to a cost function. Starting from an initial random population, points with better fitness values are used to construct a new population of solutions by means of genetic operators. Basically, these are: (i) selection, that determines which individuals survive to the next generation, (ii) crossover, that generates new chromosomes by randomly combining parts from good solutions, and (iii) mutation, that sporadically changes some bits of the new individuals. Thus, after several iterations (generations), the overall fitness value is improved by exploiting the best solutions and exploring new possibilities (Man et al., 1999).

GAs are useful for finding an optimized transformation T_k from experimental data because it is straightforward to code and evaluate the possible solutions (Martínez, 2003). Besides, the stochastic nature of this technique is valuable for coping with local minima. Thus, the genetic algorithm can find a motion estimation (Δx, Δy, $\Delta \phi$) that minimizes the fitness value I_{T_k}. Each parameter of T_k is a gene coded as a bit string. This means that the problem space has to be discretized into a finite solution space with a resolution given by the chromosome length. A complete chromosome results from the concatenation of the three genes (see Fig. 3).
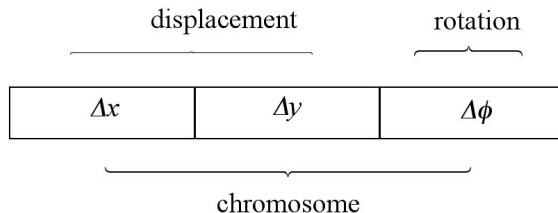

Figure 3: Genetic representation of a movement in the plane.

The tridimensional problem space is centered in the odometric estimation T_k^o, and its limits are set according to the odometric error bound $\mathbf{b}$. The finite solution space consists of all the possible chromosomes that can be codified.

For each individual of the population, this method first extracts T_k from the chromosome. Then, $\{\hat{\mathbf{q}}_k\}$ is obtained by projecting polar coordinates of $\{\mathbf{q}_{k+1}\}$ onto the XY_k frame according to Eq. (4). The correspondence function can directly be established geometrically as (see Fig. 2):

$$J(j) = \text{round}\left(\frac{\hat{\alpha}_k(j)}{\rho}\right) \tag{17}$$

9

The matching error function $e_{T_k}(j)$ of Eq. (5) is computed as the difference between the actual and the projected ranges:

$$e_{T_k}(j) = \begin{cases} E, & \text{if } (J(j) < 0 \text{ or } J(j) > N) \text{ and } \Phi < 360° \\ |d_k(J(j)) - \hat{d}_k(j)|, & \text{otherwise} \end{cases}$$

(18)

Note that with partial field-of-view scanners (i.e., $\Phi < 360°$), Eq. (17) renders some non valid indexes when $\Delta\phi$ is not null. The match error assigned to these cases is the correspondence threshold E that results in $p_{T_k}(j) = 0$ when evaluating Eq. (6).

The threshold E is a constant distance for all the genetic search, whose value is an upper bound of the expected odometric errors:

$$E = \sqrt{b_x^2 + b_y^2}$$

(19)

Finally, the expression of $e_{T_k}(j)$ indicated in Eq. (18) is employed to compute Eq. (9) as the fitness value of each chromosome for the genetic tournament.

2.3 Hybrid GA-ICP method

Previous theoretical study as well experimental analysis (which, for the sake of clarity is discussed in the next section) evidence that the combination of ICP and GA methods can be a promising solution to the motion estimation problem. Such combination would benefit from the robustness of GA to cope with local minima as well as from the efficiency of ICP's direct search. Therefore, in this section we propose a new hybrid GA-ICP method for mobile robot motion estimation. Interestingly, another combination of ICP with a random search procedure (in particular, Simulated Annealing) has been reported for the case of 3D surface registration (Luck et al., 2000).

The hybrid approach consists of a two-step algorithm:

1. GA performs a complete but rough search around the odometric estimation T_k^o that avoids local minima. This is accomplished by defining a shorter bit string for each gene but maintaining the limits of the problem space. In this way, the size of the solution space is reduced, as well as running time. Hence, the GA search results in a coarse transformation T_k^{GA}.

2. Then, the ICP technique starts from T_k^{GA} instead of T_k^o in order to refine the coarse transformation with a local search. In this case, the maximum expected initial error E_{max} has a lower bound. This reduction of search uncertainty favours fewer iterations for ICP convengence.

Thus, the new laser-point matching method for mobile robot motion estimation profits from the exploration capabilities of GA and from the refinement of ICP at a reasonable running time cost.

3 Experimental comparison

3.1 Experimental setup

The motion estimation methods described above could be applied to any robotic vehicle equipped with a 2D laser rangefinder and dead-reckoning. In this case, the tracked mobile robot Auriga-α has been employed for outdoor experiments (see Fig. 4). The vehicle of 260 kg is powered by an on-board petrol-fed AC generator of 4 kW. The locomotion system is based on the skid-steering principle. Thus, the top speed of 1 m/s can only be reached in straight line movement and decreases to zero according to the increase in demanded curvature (Pedraza et al., 2000).

A computer based on a Pentium-IV microprocessor at 2.2 GHz governs navigation via a real-time operating system (LynxOS 4.0). Dead-reckoning is obtained by encoders on both traction motors every 30 ms. Because of skid-steering, odometric estimations in tracked vehicles are intrinsically poor, although they have been improved by using an asymmetric kinematic model (Martínez et al., 2005). An upper bound for the odometric error has been estimated to be proportional to the scan period τ:

$$b = (b_x,\, b_y,\, b_\phi) = (0.13\,\text{m/s},\, 0.13\,\text{m/s},\, 6.3°/\text{s})\,\tau \qquad (20)$$

The laser device is a conventional time-of-flight range scanner (Sick LMS 200). It has the following features: field of view $\Phi = 180°$, angular resolution $\rho = 0.5°$ (i.e., $N = 360$), and range resolution of 1 cm. A complete new scan takes 0.27 s to be transmitted to the on-board computer, although it is acquired in just 27 ms. According to the manufacturer's specifications, with a exploration horizon of 20 m, the range errors are ±4 cm. Assuming a normal distribution (Ye and Borenstein, 2002), this value corresponds to $\sigma = 1.4$ cm approximately.

The laser scanner is mounted at the front of the vehicle, 0.5 m ahead of its geometric center and 0.55 m above the ground (see Fig. 4). The scan plane is parallel to the motion plane, with the sensor Y axis aligned with the forward motion direction. Since the position of the laser does not coincide with the vehicle's center of coordinates, a fixed transformation is necessary to relate the motion estimation of the rangefinder with the vehicle's movement (Martínez, 2003).

Figure 4: The mobile robot Auriga-α.

The experiments took place in a messy alley that contains construction hardware, a builder's container, a ramp, sand humps, as well as pedestrians and cars passing through a nearby street separated by an iron gate (see Fig. 5). These objects are mostly non-structured and even mobile, which means that it is a challenging environment from the scan matching standpoint. Moreover, this environment has a hard-surface rough terrain that can be considered as approximately flat. Hence, the use of a 2D laser scan (for theoretical 2D navigation) is appropriate, but terrain unevenness introduces an additional source of uncertainty for scan matching. Auriga-α has been manually driven to record several experimental trajectories that consist of timed odometric data along with successive laser scans.

Implementation details about the motion estimators are described below. The parametrization of the methods has been set empirically based on the performance of numerous trials.

Figure 5: Experimental site.

Due to the relative low number of points in 2D scans, it is not worth using acceleration strategies to find the closest points in the ICP method. Convergence is achieved in fifteen fixed iterations. This high number of iterations for ICP is due to the use of a decremental outlier detection threshold, whose limits (given by Eqs. (15), (16) and (20)) are set as $E_{max} = 0.034\,\tau^2\,\mathrm{m}^2/\mathrm{s}^2$ and $E_{min} = 0.009\,\mathrm{m}^2$, respectively.

Regarding the GA method, each parameter has been coded into a 6-bit string, thus forming individuals of 18 bits. The boundaries of the problem space are defined by the values of **b** in Eq. (20) around the odometric estimation T_k^o. According to Eq. (19), the threshold is $E = 0.184\,\tau\,\mathrm{m}/\mathrm{s}$.

The genetic algorithm has been set to iterate 60 generations with a population size of 120 solutions. The individuals above the fitness arithmetic mean are replaced every generation. One-point crossover is applied to the parents, which are chosen randomly from the entire population. The mutation rate has been set to 1 bit per 6 new chromosomes.

For the hybrid method, the GA phase is implemented exactly as described above, except for a solution space resolution of 15 bit chromosomes (five bits per variable). This reduction of the search problem allows appropriate convergence with just 40 generations of 80 individuals. Then, the ICP step refines the coarse GA solution in just 6 iterations with the initial threshold

13

reduced to $E_{max} = 0.015\,\tau^2\,\mathrm{m}^2/\mathrm{s}^2$.

These methods have been tested by combining different values for four navigation conditions. A representative pair of each category has been considered in the paper:

- Trajectory smoothness. The 'smooth' trajectory follows an O-shaped path with an average speed of $0.2\,\mathrm{m/s}$. The 'abrupt' course is 8-shaped, with an average speed of $0.35\,\mathrm{m/s}$ and bigger accelerations and jerks. Both trajectories have approximately the same length (about $21\,\mathrm{m}$).

- Scanning angular resolution. Values of $\rho = 0.5°$ for 'high' resolution and $\rho = 1.5°$ for 'low' resolution, to process more or less points from the environment, respectively.

- Motion estimation frequency. The values of $\tau = 0.9\,\mathrm{s}$ and $\tau = 2.7\,\mathrm{s}$ have been considered to test the effect of more or less overlap between successive scans, respectively.

- Odometric accuracy. In this case, the application of either a symmetric or an asymmetric kinematic model of the vehicle (Martínez et al., 2005) allows to obtain less or more accurate odometric calculations, respectively.

Altogether, 16 different combinations of motion estimations result for each method. The metrics for the comparison include running time and accuracy.

Note that it is very difficult to know the exact history of robot poses from real motion experiments, i.e. the ground truth. Moreover, motion estimators based on laser-point matching can be very precise in the short-term, so a more accurate and expensive method such as a Kinematic GPS should be implemented in order to detect motion errors. This is why simulated scans from stationary poses are usually employed to estimate the matching errors (González and Gutiérrez, 1999), (Lu and Milios, 1997).

In our non-stop motion experiments, the robot has been forced to end near to the starting pose, so that the accumulated trajectory errors can be deduced by directly matching the first and the last scans. Particularly, the final pose error in distance e_d and the absolute value of orientation error e_ϕ are obtained in this way.

In addition, the mean value of the cost function of Eq. (9) for all the motion estimates along a trajectory provides an accuracy index. Since two definitions have been proposed for the error function, two different values can be obtained:

- I^{ICP} provides the mean matching index given $E = E_{min}$ and the ICP squared error function expressed by Eq. (12).

- I^{GA} is the mean matching index for the solution transformations T_k according to the GA error as defined by Eq. (18) with $E = 0.165\,\mathrm{m}$ (resulting from Eqs. (19) and (20) with $\tau = 0.9\,\mathrm{s}$).

Note that although the matching indexes obtained from Eq. (9) were introduced to guide iterative search in the GA and the ICP methods, the mean values defined above can be used to asses solution precision along a trajectory independently of the applied matching method.

3.2   Performance evaluation

The only navigation condition that affects running time is the angular resolution. Table 1 shows how running time increases with the number of points for the three methods (results for the intermediate case $\rho = 1°$ have also been included in the table). Besides, it can be observed that ICP is faster than the GA procedure. The advantage of ICP over GA is that in spite of the cost of computing the closest cartesian points ($1,954,815$ squared distances for $\rho = 0.5°$ and only $219,615$ for $\rho = 1.5°$), the latter is burdened by the evaluation of many chromosomes (in this case, about $2,000$ solutions have been tested regardless of angular resolution).

	$\rho = 0.5°$	$\rho = 1°$	$\rho = 1.5°$
ICP	$0.11\,\mathrm{s}$	$0.03\,\mathrm{s}$	$0.01\,\mathrm{s}$
GA	$0.29\,\mathrm{s}$	$0.14\,\mathrm{s}$	$0.11\,\mathrm{s}$
GA-ICP	$0.20\,\mathrm{s}$	$0.08\,\mathrm{s}$	$0.06\,\mathrm{s}$

Table 1: Average running time depending on angular resolution.

The table also reveals that computation demanded by GA is less dependent on the number of points than that of ICP. This is due to the GA polar correspondence, which has a linear computational complexity $O(N)$, whereas the ICP cartesian correspondence has a quadratic cost $O(N^2)$ (when applying an acceleration strategy (Zhang, 1992), it can be reduced to order $O(N \log N)$). Thus, GA takes 3 times more than ICP for the high angular resolution scenario but the rate rises to ten for the low resolution case. The hybrid approach relaxes computation requirements for both its GA and ICP steps, and it achieves a running time that averages that of the two pure methods for the three ρ values.

By replaying actual motion estimations obtained for each experimental trajectory with recorded rangefinder data, it is possible to plot maps and estimated paths. Figs. 6 and 7 show such maps for the three methods (assuming 'high' angular resolution, 'high' motion estimation frequency and accurate odometry) in the 'smooth' and 'abrupt' trajectories, respectively. The global coordinate system coincides with the sensor frame in the first scan. All laser points are shown, including outliers.

Observation of these figures allows intuitive assessment on the growth of pose uncertainty introduced by each method. Map consistency in the figure (i.e., the repeatability of scanner points in the environment contours) reveals that the motion estimation of the ICP algorithm is poorer for both trajectories, and specially for the 'abrupt' one.

Performance of the GA and the hybrid methods is quite good in terms of map consistency, and they offer similar results in view of the figures. Taking into account that the ICP has the last say in the hybrid approach, the relative lack of accuracy of its solo version can be explained by its sensibility to local minima.

These conclusions agree with a more objective analysis of the experimental data inferred by computing e_d, e_ϕ, I^{GA}, and I^{ICP} for the three techniques. The values for these indexes corresponding to the experiments shown in Figs. 6 and 7 are presented in Tabs. 2 and 3, respectively.

	e_d (m)	e_ϕ (rad)	I^{GA}	I^{ICP}
ICP	0.751	0.0357	0.0448	0.00340
GA	0.179	0.0544	0.0346	0.00164
GA-ICP	0.345	0.0272	0.0358	0.00159

Table 2: Accuracy indexes for the experiments of Fig. 6.

	e_d (m)	e_ϕ (rad)	I^{GA}	I^{ICP}
ICP	1.461	0.204	0.0645	0.00490
GA	0.209	0.095	0.0432	0.00201
GA-ICP	0.249	0.105	0.0444	0.00193

Table 3: Accuracy indexes for the experiments of Fig. 7.

The overall effects of the alternative values for each separate navigation condition are depicted in the bar diagrams of Figs. 8, 9, 10 and 11. Each side of the bars represents the mean value for the eight condition combinations that share the same category value. Note that in these diagrams, the I^{GA}
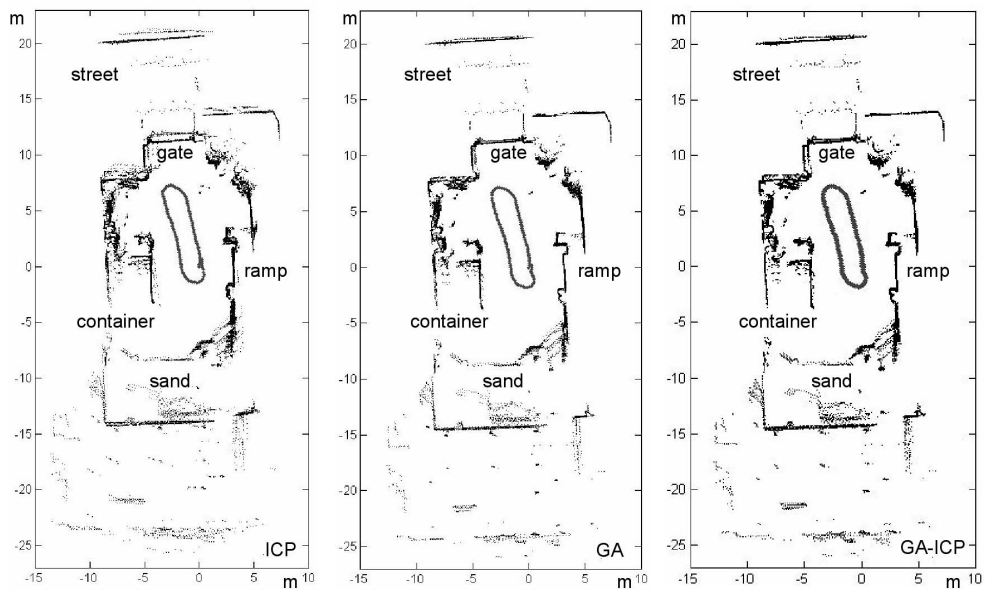
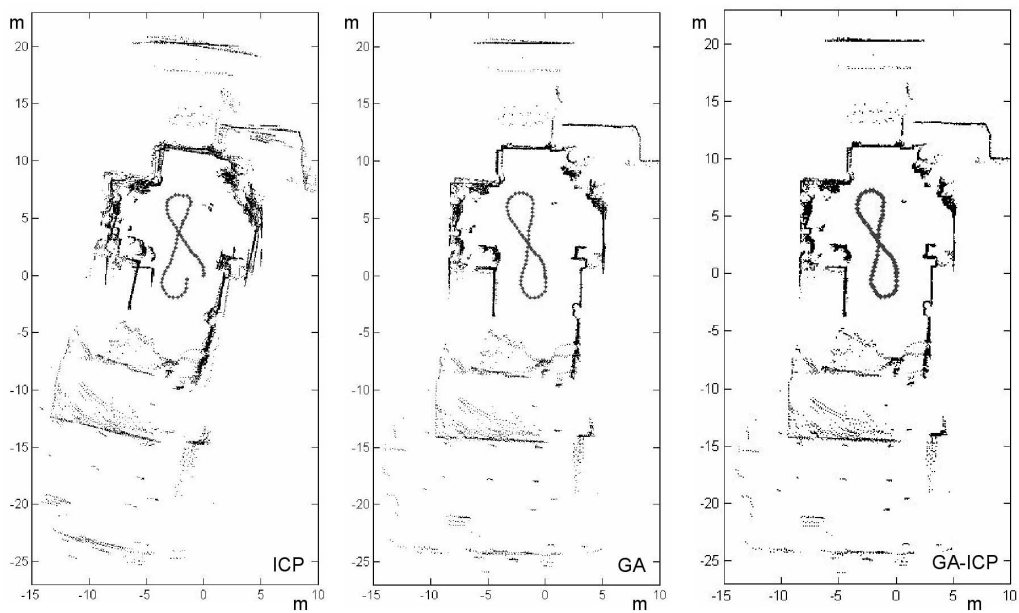Figure 6: Estimated paths and perceived maps with the ICP, GA and hybrid techniques along the 'smooth' trajectory.

Figure 7: Estimated paths and perceived maps with with the ICP, GA and hybrid techniques along the 'abrupt' trajectory.

17

and I^{ICP} values have been scaled by 10 and by 100, respectively, only for display purposes.

The most noticeable fact about these results is that GA clearly prevails over ICP in every scenario by achieving better (i.e., lesser) values in the four performance indexes. As for the GA-ICP method, the bar graphs indicate performance indexes of the same order as those of the GA. The bar graphs also show that overall performance is worse for the three methods under the most demanding conditions, i.e. 'abrupt' trajectory, less environmental information, less scan overlap, and worse dead-reckoning.

Interestingly, the hybrid approach obtains slightly better results than the GA in the I^{ICP} index due to the refinement provided by its ICP step, but this also causes I^{GA} to be a bit worse. The final position errors e_d, e_ϕ are almost the same for GA and GA-ICP.
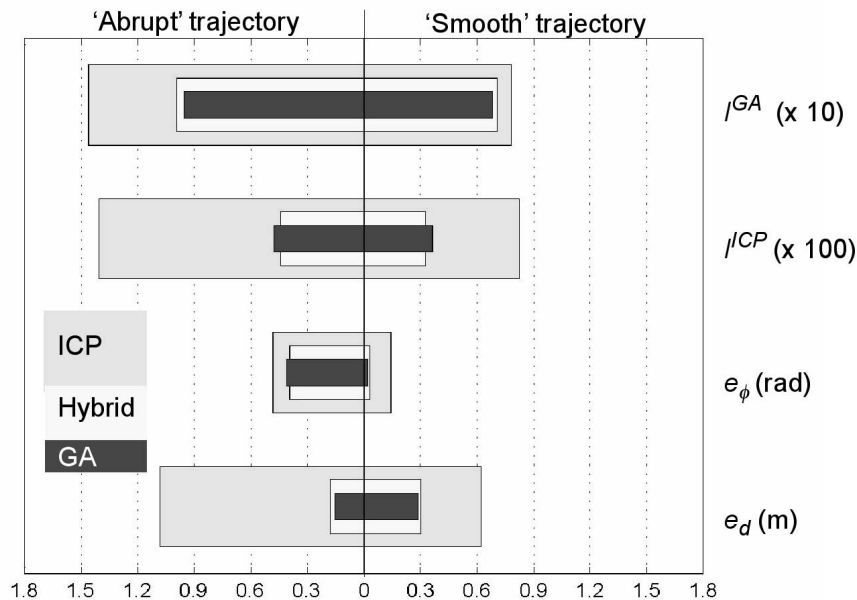

Figure 8: Bar graph of the accuracy indexes for the 'abrupt' and 'smooth' trajectories.

4   Conclusions

The paper has reported on mobile robot motion estimation methods based on point matching from successive 2D laser scans. This approach provides an ego-motion solution that is useful for navigation in unstructured and dynamic
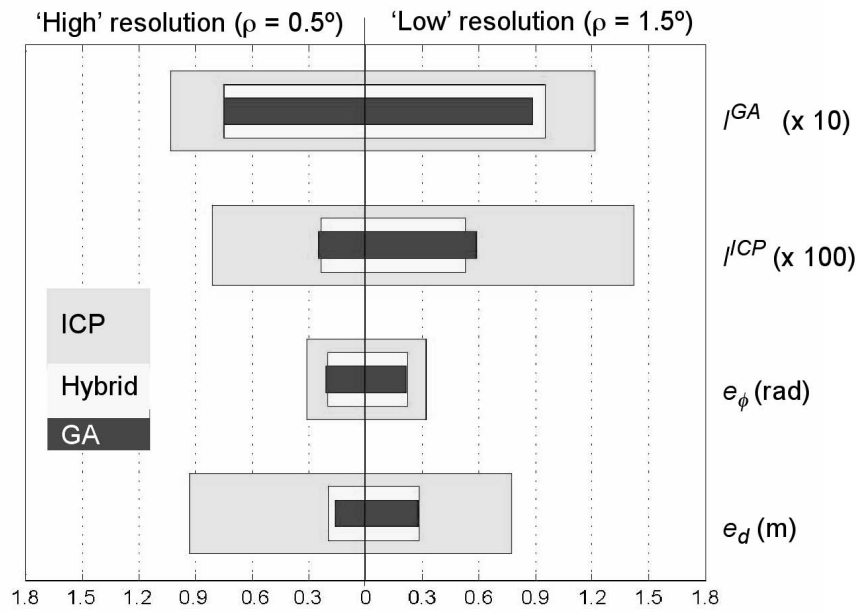
18

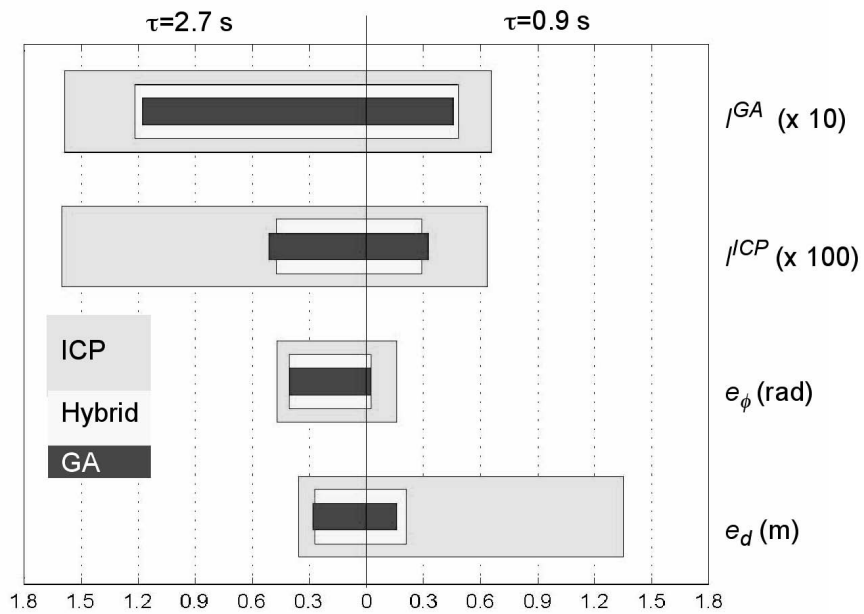Figure 9: Bar graph of the accuracy indexes for angular resolutions $\rho = 0.5°$ and $\rho = 1.5°$.

Figure 10: Bar graph of the accuracy indexes for motion estimation intervals of $\tau = 2.7\,\text{s}$ and $\tau = 0.9\,\text{s}$.
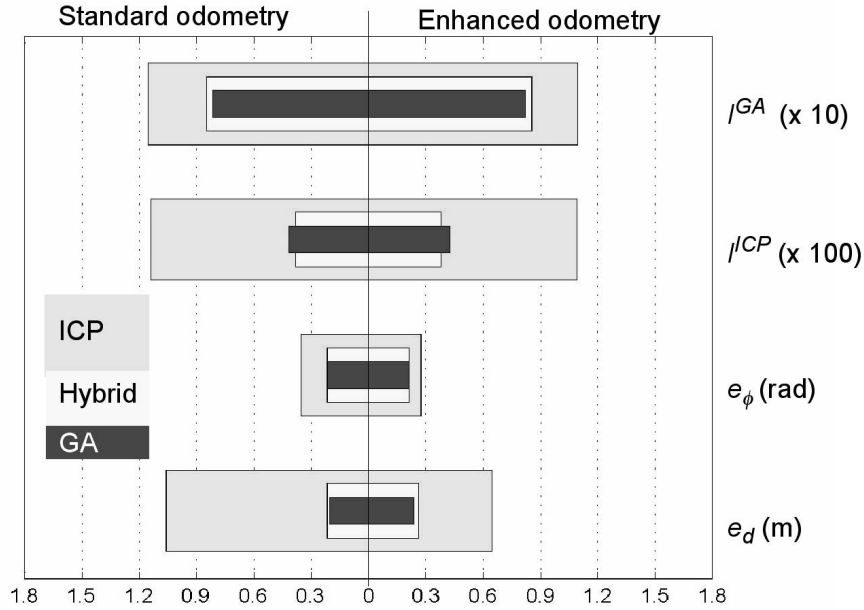
Figure 11: Bar graph of the accuracy indexes for standard and enhanced odometry.

environments, as it relies on raw sensor information rather than on extracted environmental features.

Particularly, we have analyzed two essentially different laser point matching methods, ICP and GA. Furthermore, based on that analysis, we propose a hybrid GA-ICP technique. These methods iterate starting from the odometric estimation to find a transformation that best matches two successive laser scans.

The ICP method is a local-scope optimizer that is the most popular registration algorithm for 3D surfaces. A fast 2D version of this method has been considered for ego-motion estimation. A special decremental outliers detection threshold has been devised, given that the number of laser points is smaller than in 3D applications and that these are much noisier.

The GA method is a reliable stochastic approach that constitutes a novel approach for this problem. Even though GAs are usually regarded as too computationally expensive for real time applications, the implemented GA scan matching approach provides acceptable computation time due to the application of polar correspondences of points.

The key idea behind the proposed two-phase hybrid method it to obtain a coarse motion estimation from a rough search with the GA in order to cope with local minima. Then, this solution is refined by ICP, which finds

the closest points based on this coarse estimation. The computational load of GA is lightened with respect to the pure method, since the resolution of the solution space can be conveniently reduced for the rough search. In this sense, the ICP phase requires less iterations than its pure counterpart because the initial estimation is closer to the actual solution.

These methods have been implemented and tested for the Auriga-α mobile robot in an outdoor scenario. Non-stop motion experiments have shown that ICP is a much faster method, whereas GA outstands in motion estimation accuracy. Moreover, the tested accuracy of GA-ICP parallels that of GA while its running time has been cut to an average value between the pure methods. These results have been corroborated by further experiments (not shown in the paper) in a structured indoor environment: a hall of a building which contains glass doors, columns, staircases and corridors and passers-by.

Future work will explore the identification and tracking of moving objects by further processing of the outlier points. Besides, we are interested in evaluating the performance of these techniques when applied to 3D scan matching problems for off-road navigation of mobile robots.

References

Agrawal, A., Ansari, N., and Hou, E. S. H. (1994). Evolutionary programming for fast and robust point pattern matching. In *Proc. IEEE/RSJ Int. Conf. on Intelligent Robots and Systems*, pages 1777–1782, Germany.

Besl, P. J. and McKay, N. D. (1992). A method for registration of 3D shapes. *IEEE Transactions on Pattern Analysis and Machine Intelligence*, 14:239–256.

Blais, G. and Levine, M. D. (1995). Registering multiview range data to create 3D computer objects. *IEEE Transactions on Pattern Analysis and Machine Intelligence*, 17:820–824.

Borenstein, J., Everett, H. R., Feng, L., and Wehe, D. (1997). Mobile robot positioning: sensors and techniques. *Journal of Robotic Systems*, 14:231–249.

Chen, Y. and Medioni, G. (1991). Object modeling by registration of multiple range images. In *Proc. IEEE Int. Conf. on Robotics and Automation*, pages 2724–2729, USA.

Crowley, J. L., Wallner, F., and Schiele, B. (1998). Position estimation using

principal components of range data. In *Proc. IEEE Int. Conf. on Robotics and Automation*, pages 3121–3128, Belgium.

Fitzgibbon, A. W. (2001). Robust registration of 2D and 3D point sets. In *Proc. Conf. British Machine Vision*, pages 411–420, UK.

González, J. and Gutiérrez, R. (1999). Direct motion estimation from a range scan sequence. *Journal of Robotic Systems*, 16:73–80.

González, J., Ollero, A., and Reina, A. (1994). Map building for a mobile robot equipped with a 2D laser rangefinder. In *Proc. IEEE Int. Conf. on Robotics and Automation*, pages 1904–1909, USA.

Lu, F. and Milios, E. (1997). Robot pose estimation in unknown environments by matching 2D range scans. *Journal of Intelligent and Robotic Systems*, 18:249–275.

Luck, J., Little, C., and Hoff, W. (2000). Registration of range data using a hybrid simulated annealing and iterative closest point algorithm. In *Proc. IEEE Int. Conf. on Robotics and Automation*, pages 3739–3744, USA.

Madhavan, R., Dissanayake, M. W. M. G., and Durrant-Whyte, H. F. (1998). Autonomous underground navigation of an LHD using a combined ICP-EKF approach. In *Proc. IEEE Int. Conf. on Robotics and Automation*, pages 3703–3708, Belgium.

Man, K. F., Tang, K. S., and Kwong, S. (1999). *Genetic Algorithms, Concepts and Designs.* Springer, UK.

Martínez, J. L. (2003). Mobile robot self-localization by matching successive laser scans via genetic algorithms. In *Proc. 5th IFAC Int. Symp. on Intelligent Components and Instruments for Control Applications*, pages 1–6, Portugal.

Martínez, J. L., Mandow, A., Morales, J., Pedraza, S., and García-Cerezo, A. (2005). Approximating kinematics for tracked mobile robots. *The International Journal of Robotic Research*, 24:867–878.

Muñoz, V. F., Martínez, J. L., and Ollero, A. (1994). Navigation with uncertain position estimation in the RAM-1 mobile robot. In *Proc. IFAC Int. Conf. on Artificial Intelligence in Real Time Control*, pages 215–219, Spain.

Neugebauer, P. J. (1997). Geometrical cloning of 3D objects via simultaneous registration of multiple range images. In *Proc. IEEE Int. Conf. on Shape Modeling and Applications*, pages 130–139, Japan.

Pedraza, S., Fernández, R., Muñoz, V., and García-Cerezo, A. (2000). A motion control approach for a tracked mobile robot. In *Proc. 4th IFAC Int. Symp. on Intelligent Components and Instruments for Control Applications*, pages 147–152, Argentina.

Rusinkiewicz, S. and Levoy, M. (2001). Efficient variants of the ICP algorithm. In *Proc. 3th Int. Conf. on 3D Digital Imaging and Modelling*, pages 145–152, Canada.

Shaffer, G., González, J., and Stentz, A. (1992). A comparison of two range-based pose estimators for a mobile robot. In *Proc. SPIE Conf. on Mobile Robots*, pages 661–666, USA.

Surmann, H., Nüchter, A., Lingemann, K., and Hertzberg, J. (2004). 6D SLAM-Preliminary report on closing the loop in six dimensions. In *Proc. 5th IFAC/EURON Symp. on Intelligent Autonomous Vehicles*, pages 1–6, Portugal.

Thrun, S., Burgard, W., and Fox, D. (2000). A real-time algorithm for mobile robot mapping with applications to multi-robot and 3D mapping. In *Proc. IEEE Int. Conf. on Robotics and Automation*, pages 321–328, USA.

Weber, J., Franken, L., Jörg, K. W., and Puttkamer, E. (2002). Reference scan matching for global self-localization. *Robotics and Autonomous Systems*, 40:99–110.

Weiß, G., Wetzler, C., and Puttkamer, E. (1994). Keeping track of position and orientation of moving indoor systems by correlation of range-finder scans. In *Proc. IEEE/RSJ Int. Conf. on Intelligent Robots and Systems*, pages 595–601, Germany.

Ye, C. and Borenstein, J. (2002). Characterization of a 2D laser scanner for mobile robot obstacle negotiation. In *Proc. IEEE Int. Conf. on Robotics and Automation*, pages 2512–2518, USA.

Zhang, Z. (1992). Iterative point matching for registration of free-form curves. Technical Report 1658, INRIA, France.